



OPEN

Characterization of alginate extracted from *Sargassum latifolium* and its use in *Chlorella vulgaris* growth promotion and riboflavin drug delivery

Shimaa R. Dalal¹, Mervat H. Hussein¹, Noura El-Ahmady El-Naggar^{1,2}✉, Sahar I. Mostafa³ & Sami A. Shaaban-Dessuuki¹

Alginates derived from macroalgae have been widely used in a variety of applications due to their stability, biodegradability and biocompatibility. Alginate was extracted from Egyptian *Sargassum latifolium* thallus yielding 17.5% w/w. The chemical composition of *S. latifolium* is rich in total sugars (41.08%) and uronic acids (47.4%); while, proteins, lipids and sulfates contents are 4.61, 1.13 and 0.09%, respectively. NMR, FTIR and TGA analyses were also performed. Crystallinity index (0.334) indicates alginate semicrystalline nature. Sodium alginate hydrolysate was evaluated as *Chlorella vulgaris* growth promoter. The highest stimulation (0.7 g/L biomass) was achieved by using 0.3 g/L alginate hydrolysate supplementation. The highest total soluble proteins and total carbohydrates were 179.22 mg/g dry wt and 620.33 mg/g dry wt, respectively. The highest total phenolics content (27.697 mg/g dry wt.), guaiacol peroxidase activity (2.899 $\mu\text{mol min}^{-1} \text{g}^{-1}$) were recorded also to 0.3 g/L alginate hydrolysate supplementation. Riboflavin-entrapped barium alginate-Arabic gum polymeric matrix (beads) was formulated to achieve 89.15% optimum drug entrapment efficiency (EE%). All formulations exhibited prolonged riboflavin release over 120 min in simulated gastric fluid, followed Higuchi model ($R^2 = 0.962\text{--}0.887$) and Korsmeyer–Peppas model with Fickian release (n ranges from 0.204 to 0.3885).

Marine algae are plant-like organisms that are typically found fixed on hard bases in coastal regions. They are oxygen producers, represent the food base for most of the aquatic life and represent the main source of crude oil, food, and many pharmaceutical and industrial products for humans¹. Currently, natural macroalgal-derived polysaccharides have attained more attention owing to their distinctive characteristics as stability, biodegradability in addition to biocompatibility. Seaweeds represent a promising potential source of numerous bioactive compounds as a variety of polysaccharides, phenolic compounds, pigments, vitamins, and dietary fibers that have been experimentally assessed for their biological impact of newly produced medications².

Alginate is a gelling anionic polysaccharide derived from phaeophytes. 1,4-linked-d-mannuronic (M residues) and L-guluronic acids (G residues) represent the constituents of the linear biopolymer alginate which are partitioned into homopolymeric blocks (G- and M-blocks) and heteropolymeric blocks (MG-blocks)³. The viscosity as well as gel strength of the algal polysaccharide solution are affected by the type of algal polysaccharide, temperature, pH, and presence of ions such as K^+ and Ca^{2+} ⁴. Owing to pH sensitivity of the alginate (ionotropic gelation); it shrinks in an acidic medium and swells in high pH conditions³. Berg et al.⁵ was the first to apply organic gels in drug delivery systems, then, attention has increased to use these materials in the pharmaceutical industry⁶. García-González et al.⁷ manufactured alginate in the form of aerogels, microbeads of pectin and starch and applying them as drug carriers.

Alginate oligomers could be prepared by two methods. Enzymatic digestion by alginate lyase is the most common method, producing alginate oligomers with an unsaturated terminal construction. The second method is

¹Botany Department, Faculty of Science, Mansoura University, Mansoura, Egypt. ²Department of Bioprocess Development, Genetic Engineering and Biotechnology Research Institute, City of Scientific Research and Technological Applications (SRTA-City), New Borg El-Arab City, Alexandria 21934, Egypt. ³Chemistry Department, Faculty of Science, Mansoura University, Mansoura, Egypt. ✉email: nouraalhamdy@yahoo.com

acid hydrolysis, which produce alginate oligomers with saturated terminal construction. Iwamoto et al.⁸ revealed that alginate oligomers terminal construction has a great impact on its biological reactions, they elucidated that alginate oligomers of terminal construction with double bonds exhibits greater activities than oligomers with saturated terminal construction. Oligomers are applied to promote a variety of biological and physiological activities of plants, such as seed germination, shoot elongation, root development, flower development, antimicrobial activity, heavy metal stress alleviation, phytoalexin activation², microchlorophytes growth promotion⁹.

Chlorella species are very significant for the lipids and biomass production¹⁰, adaptable to various environmental conditions¹¹, tolerant to high CO₂ concentrations¹², helpful in the treatment of industrial effluents¹³ and purification of waste-water systems¹⁴.

Alginate is amongst the most preferable biopolymeric substances used in drug delivery and encapsulation systems because it is biocompatible, biodegradable, available and affordable biopolymer¹⁵. Some bioactive constituents are incorporated within a matrix of certain formulations for attaining some activities as immobilization, protection, stabilization in addition to controlled release. Furthermore, alginate forms a thermally stable biocompatible hydrogel system in the presence of di-valent or tri-valent cations¹⁶. On the other hand, formation of alginate beads can be simply achieved by dropping of alginate solution into calcium chloride solution. The formed alginate beads are included in many capsulation applications such as biomedical, bioprocess, pharmaceutical fields in addition to food and feed industries¹⁷. Alginate applications might be significantly affected by its chemical composition, concentration, purity in addition to the valency and the concentration of the gelling cations.

Among the main innovation challenges nowadays is the encapsulation of bioactive molecules for drugs and food supplements and/or controlling their release system for improved drug bioavailability. These encapsulated hydrogel beads, after loading, can be mentioned as immobilized biocatalysts for the regulated release of the encapsulated molecules¹⁸. Being nontoxic, alginate is one of the most widely used polymers in drug delivery systems which deliver proteins and drugs, protecting them from destruction by gastric juice¹⁹. The foundation of encapsulation process is to produce a biocompatible barrier between the medium and the substrate loaded in the protective matrix¹⁶. Hydrogel matrices are cross-linked networks of natural molecules modified to attain organized release of biologically-active compounds and are affected by interaction with environmental stimuli²⁰. These hydrogels are appropriate to encapsulate hydrophilic molecules to be capable of water holding. Riboflavin (vitamin B2) is one of the hydrophilic, water-soluble bioactive molecules, it has been selected as a model drug in many studies on encapsulation and organized sustained release of hydrophilic active compounds²⁰.

The present study was designed to extract and characterize alginate derived from the Egyptian phaeophyte, *S. latifolium*, in addition to evaluation of *Chlorella vulgaris* growth criteria in response to sodium alginate hydrolysate supplementation, as well as assessing alginate blended with Arabic gum potentiality as a carrier matrix for riboflavin drug delivery in simulated gastric juice.

Results and discussion

Yield and chemical composition of the extracted sodium alginate. *Sargassum latifolium* yielded 17.5% (w/w) sodium alginate based on the dry biomass. Our results were in accordance with those obtained by Chandía et al.²¹ who reported that sodium alginate obtained from *Lessonia vadosa* was 3.0–17.7%/dry weight and Belattmania et al.²² who reported that sodium alginate yield obtained from *Sargassum filipendula* was 17% (w/w). On the other hand, Mohammed et al.²³ applied response surface to optimize the alginate extraction from *Sargassum* sp. and achieved 28% alginate yield.

Results demonstrated that 41.08% for total sugars, 47.46% for uronic acids in addition to minor contents of proteins (4.61%), lipids (1.13%), water (2%) and 0.09% for sulfates and low amounts of fucoidans were co-extracted from *S. latifolium*²⁴. The present results are in agreement with the results obtained by Larsen et al.²⁵, Duarte et al.²⁶ and Goma et al.²⁷ who documented that alginate and/or fucoidan are the main components of polysaccharide matrix in most *Sargassum* species. In accordance with our results, Viswanathan and Nallamuthu²⁸ reported that protein and lipids contents of sodium alginate derived from some seaweeds were 1.4%–7.17% and 1.76%–6.12%, respectively.

UV-visible analysis. UV-visible spectrogram of alginate extract (Supplementary Fig. S1) illustrated the assignment of absorption peak in 200–400 nm range recognizing the carboxylate and proteinaceous constituents as suggested by Osman et al.²⁹. Peaks at 264 nm, 348 and 392 nm can be contributed to the presence of phenolics as well as flavonoids and their derivatives³⁰. Data demonstrated absorption bands lies between 260 and 400 nm, which distinguish the presence of aromatic and poly-aromatic compounds comprising proteins and amino acids³¹.

Proton nuclear magnetic resonance (¹H NMR) analysis. ¹H NMR spectroscopy is a significant physicochemical method for elucidating structure of polysaccharides. Structural features of alginate are elucidated by the ¹H NMR profile (Fig. 1A) which depict the chemical shifts and single monomers and blocks characteristic to the sodium alginate fraction (Fig. 1A), revealing purity³². Data revealed the recognition of β-anomeric protons in the alginate sample in addition to appearance of protons signals within a 2-ppm chemical shift range (3 to 4 ppm). Assignments of the signs in the anomeric zone are recognized³³ whereas, 2 signals in the anomeric region were documented.

The present results illustrated Signal II corresponding to the overlap between mannuronic acid anomeric proton (M-1) and the H-5 of alternating blocks (GM-5) besides, Signals III corresponding to proton H-5 guluronic acid from the GG-5G block (G-5) in the alginate sample indicating the heterogeneous (FGM) blocks of alginate³⁴. The ¹H NMR profile revealed presence of guluronic acid H-5 (GG-5G) that was recognized at 4.282 ppm (signal III) as suggested by Usoltseva et al.³² and Flórez-Fernández et al.³⁵. Furthermore, the characteristic signals of

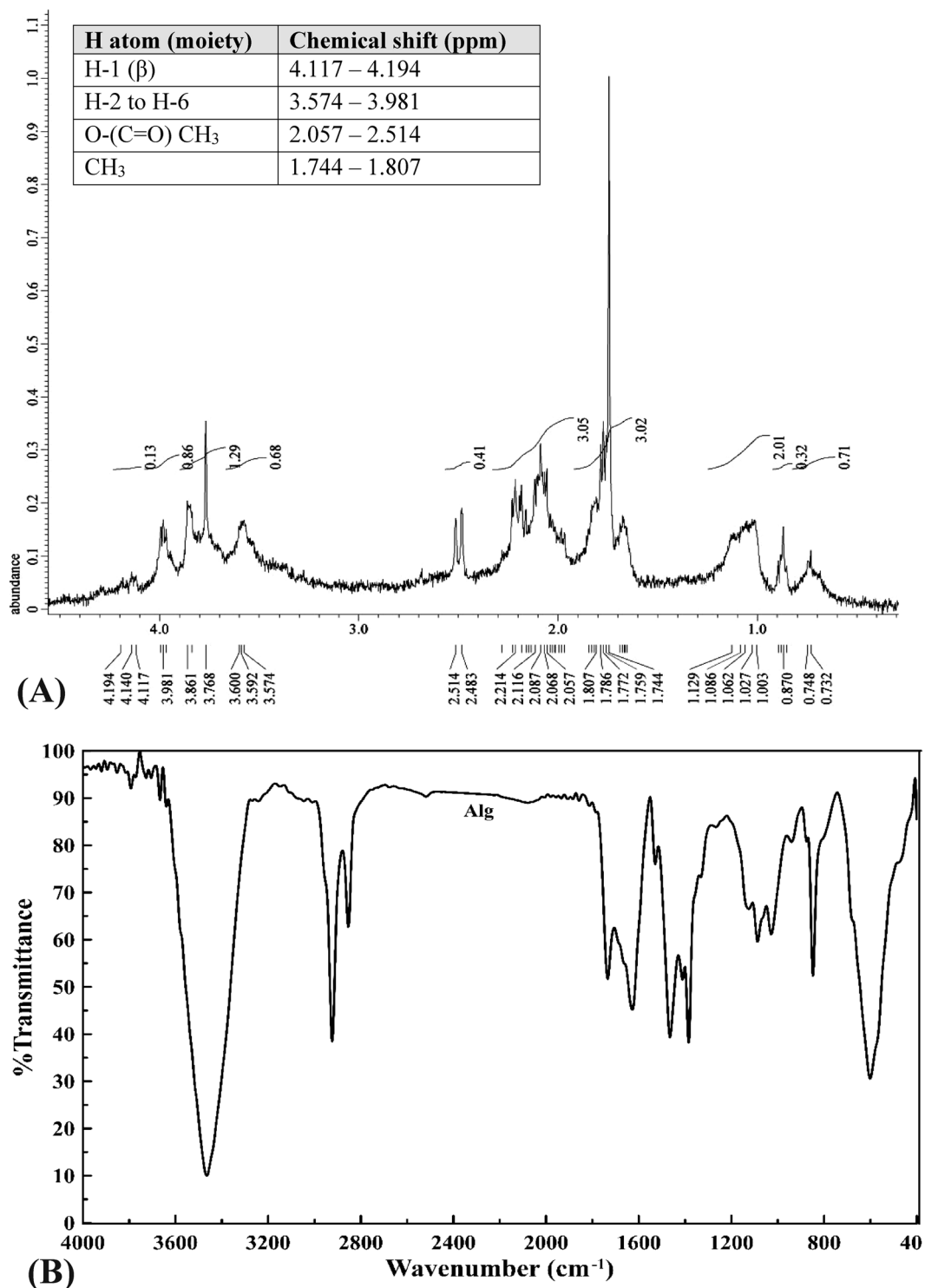


Figure 1. (A) NMR of extracted sodium alginate, (B) FTIR analysis of sodium alginate.

fucofucose at 1.744–1.807 ppm for alginate revealed presence of neutral sugars traces of fucoidans which co-extracted from brown algae as interpreted by Bouissil et al.²⁴. Moreover, the overlapping signals in the ¹H NMR could be an assignment for the structure complexity of the alginate sample³⁴. Aside from alginate extracted from *Sargassum vulgare* by Hussein et al.³¹, most *Sargassum*-derived alginate have M/G < 1 and significant magnitudes of homopolymeric block M ($\eta < 1$). The heterogeneity of alginate composition could be affected by the environmental factors²³.

FTIR Spectrum of sodium alginate. Sodium alginate FTIR profile (Fig. 1B, Supplementary Table S1) revealed different chemical functional groups. FTIR spectrogram of alginate is dominated with strong absorption broad band at 3465 cm^{-1} ascribing hydroxyl group ($-\text{OH}$ stretching). Whereas, spectral peaks allocated in the range 4000 cm^{-1} – 3400 cm^{-1} could be assigned to alcohol and acids³⁵. Strong peaks in the range of 1628 to 1428 cm^{-1} designated asymmetric and symmetric stretching vibrations that attributed to carboxylate anions (COO^-)³⁵. These significant spectral peaks could take a part in the structure elucidation of alginates recognizing the metal-carboxylate interactions according to Flórez-Fernández et al.³⁵. The spectral band around 2923 – 2854 cm^{-1} is in agreement with that obtained by Aprilliza³⁶ and are attributed to aliphatic $-\text{CH}$ stretching, and symmetrical and asymmetrical $(\text{C}-\text{H})\text{CH}_2$ stretching, beside aromatic and/or vinylic $\text{C}-\text{H}$ stretching and (CH) -anomer stretching³⁷.

FTIR spectrogram of alginate also illustrated peak of $\text{C}-\text{H}$ stretching vibrations recognizing alkanes, $\text{C}=\text{O}$ indicated carbonyl group (amide I band), COO^- stretching vibrations ascribed to carboxylate as well as $\text{C}-\text{O}-\text{C}$ stretching vibrations³⁶. Peaks attained the range of 1090 – 1030 cm^{-1} are assigned to $\text{C}-\text{O}$ stretching of pyranosyl ring, $\text{C}-\text{O}-\text{C}$ asymmetric stretching (glycosidic linkage), $\text{C}-\text{C}$ stretching which are attributed to alginate saccharide structure³⁸. Also, the stretching of $\text{C}=\text{O}$ group was documented at 1734 cm^{-1} as reported by Carpenter and Saharan³⁹. The present results are in accordance with those of Cardenas-Jiron et al.⁴⁰ and Bouissil et al.²⁴. According to Gomaa et al.²⁷, the spectral band 848 cm^{-1} confirms the presence of sulfate groups of fucoidan. Peaks around 600 cm^{-1} could be due to symmetric and asymmetric $\text{O}=\text{S}=\text{O}$ deformation as reported by Flórez-Fernández et al.³⁵.

Thermogravimetric analysis (TGA). The thermal behavior of alginate (Fig. 2A) indicated mass progressive decreasing pattern with increasing temperature, demonstrating four distinctive decomposition stages characterized by temperature range for each of them. The first stage began with weight loss of 10.67% in the temperature range 49.74 – $66.68\text{ }^\circ\text{C}$, followed by a 24.90% mass loss in 245.13 – $296.99\text{ }^\circ\text{C}$ temperature range. Thereafter, 11.54% mass loss has documented in the temperature range 532.39 – $566.69\text{ }^\circ\text{C}$, ended with 8.97% mass loss within temperature range 649.02 – $659.01\text{ }^\circ\text{C}$. Under progressive elevating temperature, sodium alginate exhibited initial dehydration process during the first stage. The initial dehydration followed by two decomposition stages characterized by the production of carbonaceous residue. The decomposition stages followed by production of sodium carbonate with 40.91% carbonized matter residue at the end of the experiment which is degraded gradually according to the interpretation of Guedes Soares et al.⁴¹, exhibiting good thermal stability. The present thermal degradation behavior of sodium alginate is in agreement with those of Rani et al.⁴² and dos Santos Araújo et al.⁴³. On the other hand, Xu et al.⁴⁴ reported the thermal stability of calcium alginate capsules up to $160\text{ }^\circ\text{C}$.

X-ray diffraction (XRD). The XRD pattern was used to investigate the micro structural features of *Sargassum latifolium*—derived sodium alginate (Fig. 2B). The XRD profile illustrates three distinctive intensive crystalline diffraction, which observed at 2θ degrees values of 20.51, 21.04 and 29.73 with inter planar spacing (d -spacing) of 4.328 Å, 4.22 Å and 3.003 Å, respectively indicating a rather amorphous structure. The obtained diffractogram demonstrate crystallinity index of 0.334 indicating the semi-crystalline nature of this sodium alginate sample⁴⁵. Furthermore, owing to the interpretation of Kanimozhi et al.⁴⁶ the peak height intensity and the degree of crystallinity could diagnose the amorphous nature of alginate. In accordance with our results, Aprilliza³⁶ reported that sodium alginate extracted from brown algae has a semi-crystalline structure.

Rheological measurement. Rheological characteristics are significant parameters for the biotechnology issue of phycocolloids. The apparent viscosity of sodium alginate fraction in aqueous solutions (5, 10 and 15 mg/mL) was quantified as a function of shear rate in the range 20 – 500 s^{-1} that is illustrated in Fig. 3. Flow profile demonstrated that 40 s^{-1} shear viscosity giving maximum values of viscosity 8.03, 12.1, 22.1 centipoise (cP); respectively (Fig. 3A). At the maximum shear rate used (500 s^{-1}), the viscosity exhibit marked decrease in all alginate concentrations to 2.3, 5.1, 11.2 cP; respectively designating a shear thinning behavior⁴⁷. Non-Newtonian flow is studied via gathering the viscosity data covering the range of shear rates used to perform a rheogram representing viscosity versus shear rate. Despite the suggestion of Wildemuth and Williams⁴⁸ about the presence of conflicting issue of the distinctive shear-thinning fluids that displays an area of Newtonian flow at shear rate extremes, the present data did not illustrate any Newtonian flow behavior for the studied alginate solutions. According to the findings of Shyamali⁴⁹, *Sargassum* species—derived alginates include a higher quantity of guluronic acid blocks which yielded strong gels relative to that derived from *Macrocystis*. The detected shear-thinning pseudoplastic performance, which is considered as an irreversible structural disturbance, and the reduction of viscosity takes place due to molecular arrangement which occurs in the structural rearrangement as indicated by Glicksman⁵⁰. Flow curves of different concentrations of alginate (Fig. 3B) exhibited decreases in shear stresses showing a restrictive stable value at reduced values of shear rate designating limited yield stress of these solutions. Though greater yield stress levels could be reached with the high concentrations of alginate. The pseudoplastic property showed as shear thinning of alginate solutions is illustrated in Fig. 3C. The highest viscosity levels as well as the marked shear thinning behavior were documented to the highest concentration ending with the smallest mg alginate/mL. Rheogram (Fig. 3D) torque percent increases with increasing spindle speed (RPM). Figure 3E explains viscosity of alginate aqueous solutions & spindle speed (RPM) relationship. It is obvious that viscosity range is inversely proportional to the rotational speed. According to Truus et al.⁵¹ alginate viscosity of *Fucus* is comparatively low depending on the gathering time and drying processes of seaweeds, whereas rheological properties of alginate are temperature dependent process. Generally, a reduction in viscosity is often noticed after increasing shear rate, whereas increasing alginate concentrations induced viscos-

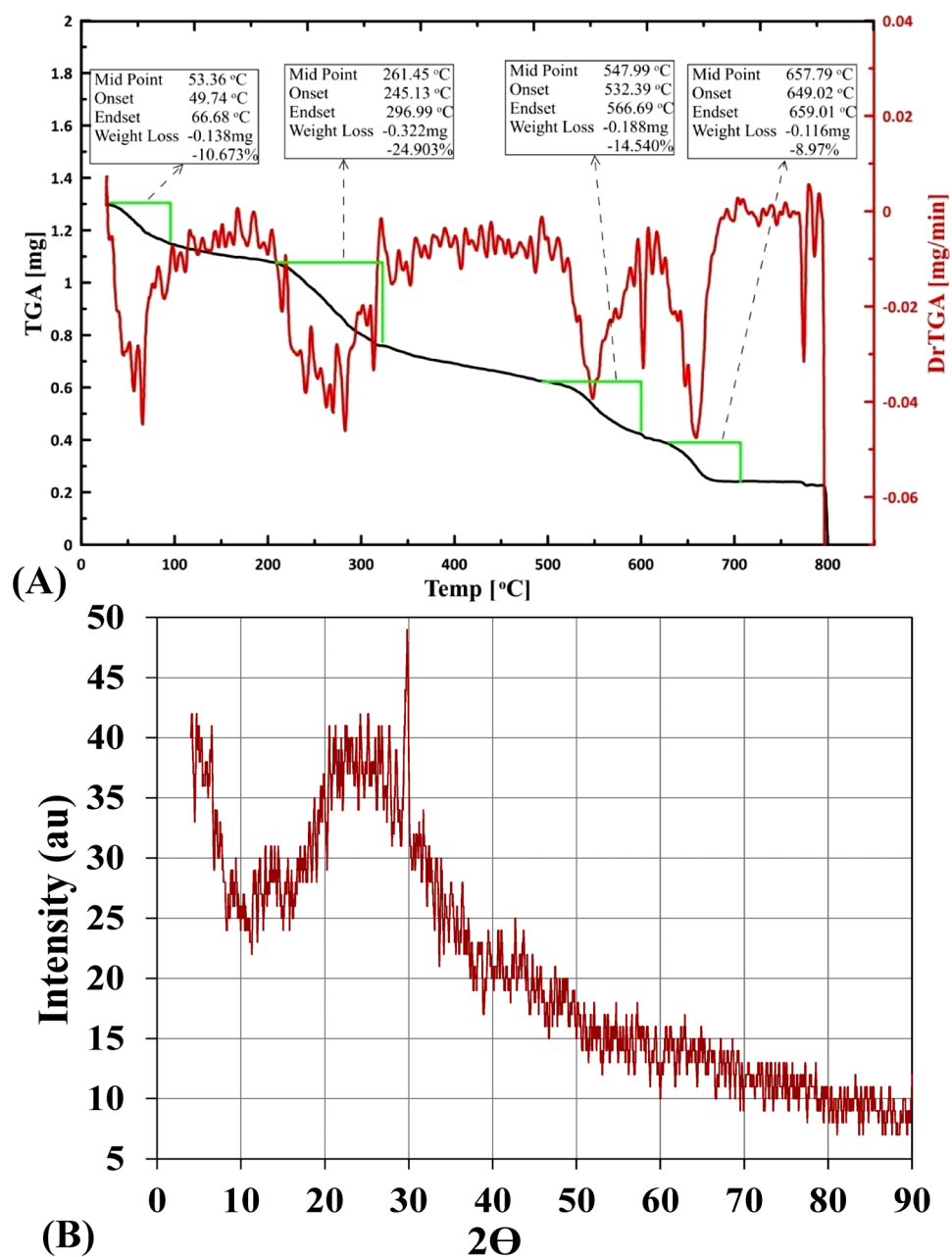


Figure 2. (A) Thermogravimetric analysis (TGA), (B) X-ray diffraction of extracted sodium alginate.

ity increments. This rheological behavior demonstrates typical non-Newtonian pseudoplastic pattern on shear thinning characterization in solutions as suggested by Picout et al.⁵² This viscosity performance was illustrated by polysaccharides of other algae⁵³. The dynamic viscosity manners of alginate polymer are influenced by both polymer structure and mass⁵⁴. Shear thinning pattern of the extracted alginate may be contributed to the hydrodynamic potential resulted throughout the shear decline of alginate structural units⁵⁵. Sutherland⁵⁶ reported that polysaccharide characterized by this rheological pattern can be incorporated into many food industries to modify dynamic viscosity behavior of the present water, changing product texture according to their gel formation ability.

Growth responses of *C. vulgaris* to alginate hydrolysate supplementation. Different alginate hydrolysate supplementations (0, 0.05, 0.1, 0.3 and 0.5 g/L) induced various levels of promoting effects on *Chlorella vulgaris* growth and metabolism over 14 days incubation period as can be seen in Fig. 4 A. All the trials were performed in triplicate in order to minimize errors and to calculate standard deviation. As shown in Fig. 4 A, *C. vulgaris* growth curve exhibits an exponential phase from the 2nd day till the 12th day after which the growth tends to be in the stationary phase. Significant increments in dry biomass (Fig. 4B), specific growth rate (Fig. 4C), protein and carbohydrate contents (Fig. 5B), total phenolics (Fig. 5C) as well as guaiacol peroxidase (Fig. 5D) over the

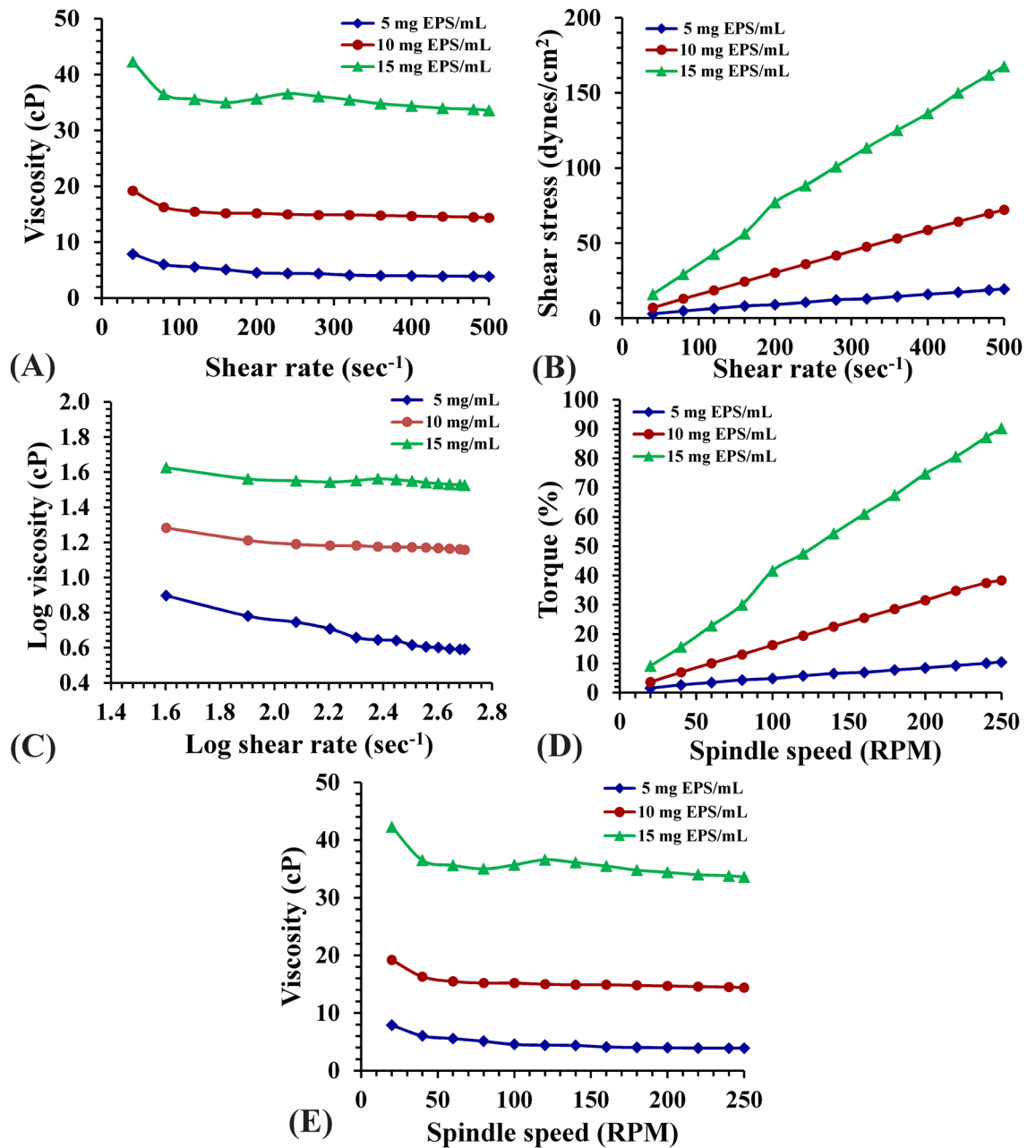


Figure 3. (A) Viscosity as a function of shear rate, (B) Flow curve of the shear stress vs. shear rate, (C) Log–log plot of the viscosity vs. shear rate, (D) Rheogram of the Torque vs. spindle speed and (E) Rheogram of the viscosity dependence of spindle speed (RPM) of aqueous solutions of extracted sodium alginate at concentrations 5, 10 and 15 mg Alg/mL.

control experiments were documented. On the other hand, all alginate supplementations decreased chlorophyll a and b contents below the control experiment while carotenoids content increased from 0.071 to 0.232 mg/g dry biomass with increasing the alginate supplementation from 0 to 0.5 g/L (Fig. 5A). In general, under this mixotrophic nutritional mode, *Chlorella vulgaris* demonstrated marked increases in most measured growth parameters, whereas, the magnitude of response followed dose response manner. The maximum stimulatory effect was induced by 0.3 g/L alginate hydrolysate supplementation for dry biomass, protein, carbohydrate contents recording values of 0.7 g/L, 179.222 mg/g dry weight and 620.332 mg/g dry biomass; respectively. Higher sodium alginate hydrolysate dose (0.5 g/L) induced nonsignificant increments in the dry biomass, protein and carbohydrate content recording 0.32 g/L, 131.215 mg/g dry weight and 433.143 mg/g dry weight; respectively. On the other hand, the specific growth rate increased in a dose–response manner, taking the bell shape response, achieving the maximum result (0.104 g/L/d) with 0.3 g/L alginate supplementation as illustrated in Fig. 4C.

Figure 5C demonstrated the induced changes in the total phenolic content of *chlorella vulgaris* under this mixotrophic mode of nutrition. Data revealed significant increases in total phenolic contents relative to the control level with increasing alginate hydrolysate concentration (18.315, 20.79, 27.697 and 26.468 mg/g); respectively.

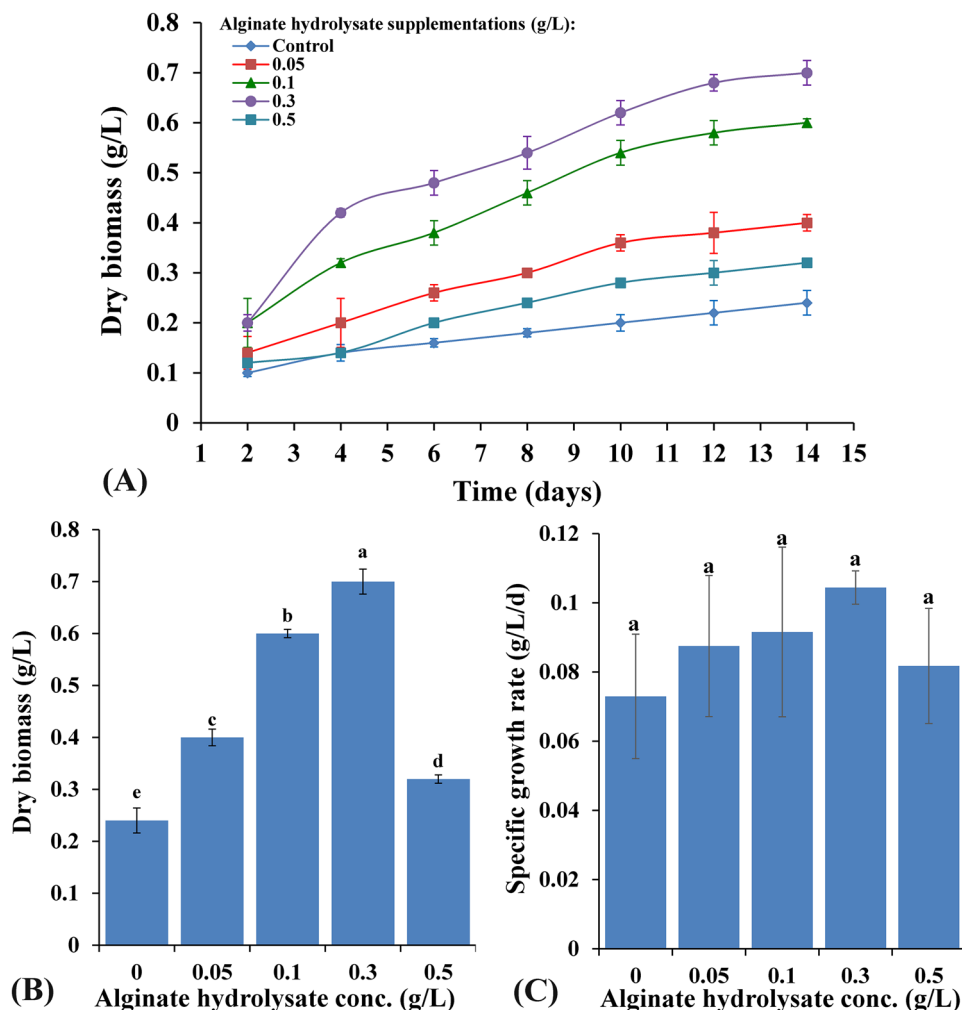


Figure 4. (A,B) Variation of *C. vulgaris* biomass content (mg/g dry wt) with different alginate hydrolysate supplementations (g/L) and (C) Variation of *C. vulgaris* specific growth rate (g/L/d) with different alginate hydrolysate supplementations (g/L).

Guaiacol peroxidase (GPX) is a key enzyme in regulation of the intracellular H_2O_2 equilibrium by transforming H_2O_2 into H_2O along with regeneration of $NADP^+$. Data of GPX activity demonstrated significant increases above the control level in concentration depending manner (1.16, 2.059, 2.899 and 2.632 $\mu\text{mol min}^{-1} \text{g}^{-1}$; respectively) as illustrated in Fig. 5D. Thereby, guaiacol peroxidase exhibited significant increases with increasing alginate hydrolysate concentration, displaying maximum activity with 0.3 g/L alginate hydrolysate treatment (2.899 $\mu\text{mol min}^{-1} \text{g}^{-1}$).

Shen et al.⁵⁷ revealed that *Chlorella vulgaris* could grow under different nutritional modes, especially the mixotrophic condition which could induce higher biomass than autotrophic and heterotrophic cultures. Furthermore, substrate concentration and external carbon source, induced final biomass of the mixotrophic cultivations while the lipids content remains unchanged. Many previous studies documented that alginate oligomers have growth promoting effect on higher plants, since *C. vulgaris* is a photosynthetic eukaryotic cell, having structural and functional similarities with higher plant cells so it responds to alginate oligomers in a comparable manner⁵⁸. Yamasaki et al.⁵⁹ demonstrated that alginate oligosaccharides may function as growth enhancing agents for certain plant cells and some green algae. In accordance with the present results, Yokose et al.⁶⁰ indicated that oligoalginate preparations provided by enzymatic hydrolysis using bacterial alginate lyase, improved growth of *Nannochloropsis oculata*. Whereas, generally, 20 mg/L oligoalginate preparations induced the optimal growth. On the other hand, they found that 40 mg/L slightly decreased the observed growth enhancing activity. As manuronic acid and guluronic acid are the main components of alginate, it may produce complex with Ca^{2+} and overcome Cu^{2+} induced growth suppression of *N. oculata*⁶⁰. Diatom *Chaetoceros gracilis* also responded positively to oligoalginate preparation except for diatom genus *Skeletonema* sp., demonstrating a species-specific growth-enhancing significance of the oligo-alginate preparation in microalgae as previously suggested by Yokose et al.⁶⁰. In the present study, alginate hydrolysate concentrations are effective on *C. vulgaris* growth and metabolism in a concentration dependent manner with a bell shaped profile. It can be observed that control experiment (0 g/L alginate hydrolysate) achieved 0.24 g/L biomass whereas the optimum growth (0.7 g/L) was achieved at 0.3 g/L

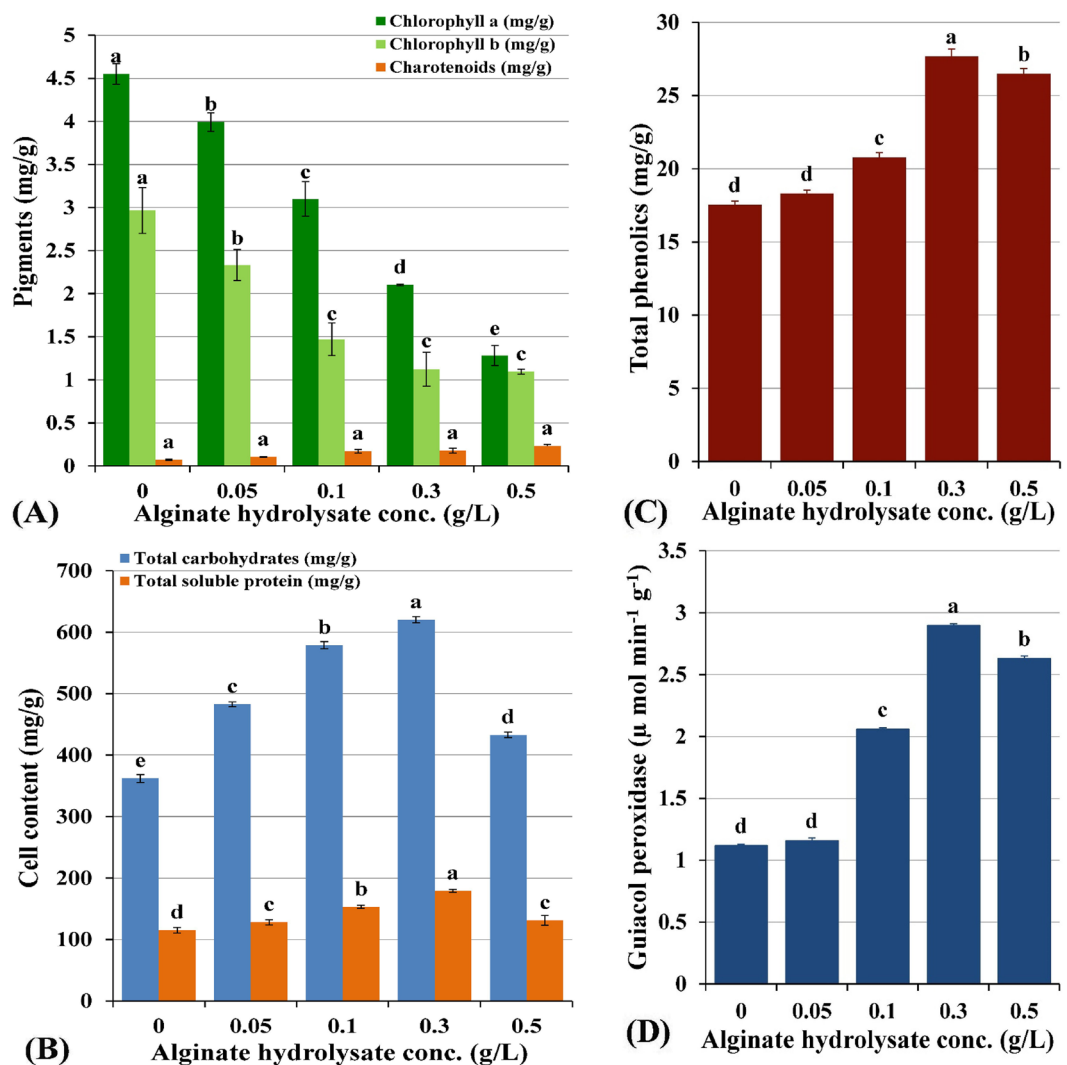


Figure 5. (A) Variation of *C. vulgaris* pigments content (mg/g dry wt.), (B) Variation of carbohydrates and protein content (mg/g dry wt.) with different alginate hydrolysate supplementations (g/L), (C) Variation of *C. vulgaris* phenolics content (mg/g), (D) guaiacol peroxidase content ($\mu\text{mol min}^{-1}\text{g}^{-1}$) with different alginate hydrolysate supplementations (mg/L).

alginate hydrolysate supplementation representing 291.67% of control growth. On the other hand, Ueno and Oda⁶¹ studied the effect of alginate oligomers different concentrations on *Chaetoceros gracilis* (0–1 mg) achieving 140% of control growth when using 0.125 mg/mL alginate oligomers supplementation. On contrast, alginate oligomers have no significant impact on *Skeletonema* sp. growth.

Moreover; 1 mg/L alginate oligosaccharides produced via alginate lyase decomposition, promoted *Chlamydomonas reinhardtii* growth. Moreover; the alginate oligomers produced after acid hydrolysis had no growth-enhancing potentiality as documented by Schafer et al.⁹. Also, increments in C16:0, C18:2, and C18:3 fatty acids content of *C. reinhardtii* were noticed after treating with enzyme-decomposing oligo-alginates excluding C18:0 level. On the other hand, acid hydrolysis produced oligo-alginates with no influence on fatty acid content as reported by Schafer et al.⁹. Thus, the oligo-alginate mixture induces the growth of microchlorophytes and increases the content of fatty acids, which may have future prospective in the biotechnological practices for biodiesel production.

According to Naeem et al.⁶², the administration of the depolymerized form of irradiated sodium alginate (ISA) as a fertilizing agent resulted in a significant increase in photosynthetic parameters, chlorophyll and carotenoids content as well as growth promotion of *Mentha arvensis*. They supposed that ISA might enable plants to catch more light energy for increasing photosynthesis and/or improving chlorophyll and carotenoids contents consequently after foliar application of ISA as documented by El-Chaghaby et al.⁶³ previous study. Moreover, when sodium alginate oligomers functioned as plant growth enhancers, they might stimulate plant vegetative growth leading to increased plant productivity relative to control⁶⁴. Degraded alginate (oligosaccharides) induced cell signaling resulted in enhancing different physiological processes in plants⁶⁵. Chlorophyll is one of the cellular compounds on the basis of which microalgal biomass in the culture is estimated and it can be used to measure cell

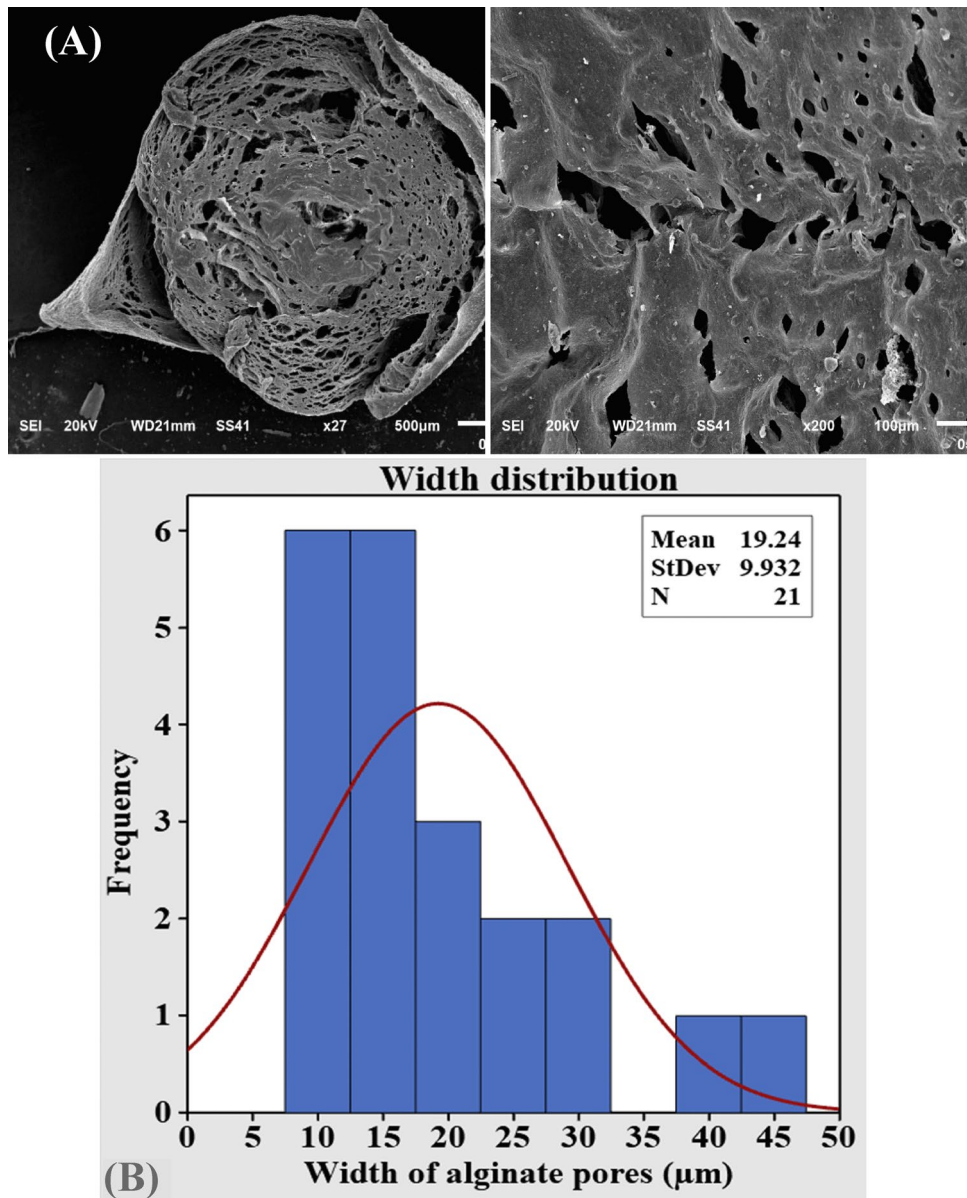


Figure 6. (A) SEM electron micrograph of alginate at different magnifications showing alginate pores, (B) width ranges of alginate pores versus its frequency,

growth. In accordance with our results, Farmer et al.⁶⁵ reported that external organic carbon source supplementation may affect photosynthesis and respiration. Also, oligomers produced by alginate depolymerization stimulates the growth and promote the germination and shoot elongation in plants⁶³. In accordance with our data, plant growth induction was achieved by the use of radiated sodium alginate oligosaccharides. Gamma irradiation of sodium alginate influences all polymer cross-linking manner, its use affects the biological activities of plant cells⁶⁴.

Scanning electron microscopy (SEM). Alginate as a smart matrix for riboflavin delivery systems was scanned using SEM. The surface and cross-sectional scanning electron microscopy images of the prepared barium alginate beads are illustrated in Fig. 6A. The dry prepared beads were virtually spherical with a mean diameter of 2.37 mm with rough surface. The cross-sectional SEM images demonstrated many closed pores with varying diameters (mean value 19.24 to 166.4 μm) (Fig. 6B). In accordance with the current results, Malakar et al.⁶⁶ reported that SEM photographs of liquid paraffin entrapped calcium alginate bead surface showed a rough surface with small pores or channels and no drug crystals were found on the bead's surface, revealing the dispersion of drug crystals in the alginate matrix. Moreover, Rashidzadeh et al.⁶⁷ reported that SEM images of alginate/Ag/Fe₃O₄ hydrogel beads are illustrated a clear rough and flat surface.

Alginate bead Formulations	EE (%)	Kinetic parameters								
		Zero-order kinetics		1st-order kinetics		Higuchi model		Korsmeyer-Peppas model		
		K_0	R^2	K_{1st}	R^2	K_H	R^2	K_p	R^2	n
F1	82.81	4×10^{-7}	0.882	4×10^{-7}	0.882	5×10^{-6}	0.962	11×10^{-6}	0.978	0.389
F2	87.76	2×10^{-7}	0.777	10^{-7}	0.792	2×10^{-6}	0.895	16×10^{-6}	0.943	0.251
F3	89.15	10^{-7}	0.791	2×10^{-7}	0.777	3×10^{-6}	0.887	17×10^{-6}	0.948	0.204

Table 1. In vitro riboflavin release encapsulation efficiency and kinetic parameters.

FTIR characterization of different sodium alginate bead formulations. FTIR spectra of sodium alginate, Arabic gum, riboflavin, Arabic gum-entrapped barium alginate beads loaded with riboflavin (F1, F2 and F3) and Arabic gum-entrapped barium alginate beads (F4, F5 and F6) are documented in Supplementary Figure S2A,B and Supplementary Table S1. FTIR analysis was applied to investigate the entrapment and stability of R in Alg-AG in the preparations (F1, F2 and F3) with different alginate and Arabic gum concentrations. FTIR profile of sodium alginate (Alg) revealed different chemical functional groups illustrated in Supplementary Fig. S2A. Spectral peaks ranged from 4000 to 3400 cm^{-1} could be assigned to -OH functional group⁶⁸, where FTIR spectrogram of alginate is dominated with strong absorption broad band at 3465 cm^{-1} ascribing hydroxyl group (-OH stretching). The peaks lying in the range of 1060–1030 cm^{-1} (C–O–C stretching) are attributed to the alginate saccharide structure. However, Sinha et al.⁶⁹ suggested that guluronic units were recognized at spectral band at 1030 and 1093 cm^{-1} wave number where the mannuronic signals were recognized. The existence of signal peaks around 1628 and 1428 cm^{-1} designating asymmetric and symmetric stretching vibrations of carboxylate anions (COO⁻)³⁵. The spectral band at 2923 cm^{-1} can be attributed to -CH chemical group³⁷. FTIR spectrogram of alginate illustrated peak of C–H stretching vibrations recognizing alkanes at 2923 cm^{-1} , C=O indicated carbonyl group (amide I band) at 1734 cm^{-1} and COO⁻ stretching vibrations ascribed to carboxylate as well as C–O–C stretching vibrations at 1628 cm^{-1} ³⁶. Furthermore, spectral peaks in the range of 848–949 cm^{-1} (C–O) stretching vibration designating the presence of mannuonic and uronic acids; respectively⁷⁰. There are weak interaction between alginate and riboflavin in all alginate-riboflavin mixtures as reported by Aprilliza³⁶.

The FTIR profile of alginate and riboflavin-encapsulating alginate Arabic gum composite (Supplementary Fig. S2B) demonstrated some variations in the intensity of peaks especially in the characteristic range 1500 to 400 cm^{-1} . These variations recognize the deformations of bonds in the region of carbohydrate. Concerning alginate beads encapsulating riboflavin, (Supplementary Fig. S2B) showed characteristic broad bands in the range of 4000 to 3100 cm^{-1} designating stretching vibration of O–H group as well as the C = C aromatic group of both alginate riboflavin, in addition to presence of C = O ketonic group of riboflavin⁶⁸ which designate stability of riboflavin in the formed beads.

According to Hosseini et al.⁷¹, the characteristic chemical groups of riboflavin are demonstrated in lower intensities and may be obscured by other signals confirming the existence of electrostatic interactions between the blend components. FTIR charts of Arabic gum-entrapped barium alginate beads loaded with riboflavin exhibited comparable features indicating absence of interference between R and Alg-AG ingredients besides non-participation of the ketonic carbonyl in coordination with alginate binding centers⁷².

For Alg-AG-R physical interaction characterization, the R carbonyl stretching region (1730–1620 cm^{-1}) was analyzed. The present data illustrated that characteristic acid carbonyl stretching band of the pure drug appeared unchanged in the polymer/drug physical mixtures, and the spectra seemed to be the sum of the spectra of the pure components.

Riboflavin encapsulation efficiency of the prepared riboflavin alginate-Arabic gum beads. Sodium alginate has the ability to form rigid gels with divalent cations. Although it is relatively easy to describe alginates in terms of M and G units, the detailed molecular compositions of alginates in terms of block lengths and block distributions are more difficult to determine. The formation of riboflavin-entrapped barium alginate beads is a simple and significant process for drug delivery. Riboflavin encapsulation efficiency of the prepared riboflavin alginate-Arabic gum beads ranged from 82.81 to 89.15% (Table 1, Fig. 7A) according to the formulation composition of the beads. The highest encapsulation efficiency was positively correlated to the Arabic gum concentration which was observed in Alg-AG-R 0.2 formulation. This pattern of response could be attributed to the partitioning of certain amounts of riboflavin in the Arabic gum phase and/or constitution of an Arabic gum barrier that prevents external passage of riboflavin molecules throughout preparation. Whereas, the physical interaction and/or enlargement of the complicated cross-linked barium alginate network may facilitate the entrapment of the drug (riboflavin) according to the interpretation of Malakar et al.⁶⁶. Results of Azad et al.⁷³ are in line with the current results whereas, they documented that the EE% of black seed oil in alginate beads ranged from 67.20 to 104.50% and increased with increasing voltage and flow rate. The encapsulation efficiency was found to be dependent on the encapsulating matrix's strength⁷⁴. On the other hand, the cross-linking ability of alginate may be able to increase the encapsulation efficiency of oil in alginate⁷⁵.

In vitro release studies. The in vitro prolonged, sustained release profile (Fig. 7B) of Alg-AG-R with different alginate-Arabic Gum composite-riboflavin formulations could be designated as two-step biphasic process. Concerning Alg-AG-R 0.1, the first phase continued for 70 min which designated by burst release, followed by a stationary phase, whereas in Alg-AG-R 0.15 and Alg-AG-R 0.2 formulations the exponential R release con-

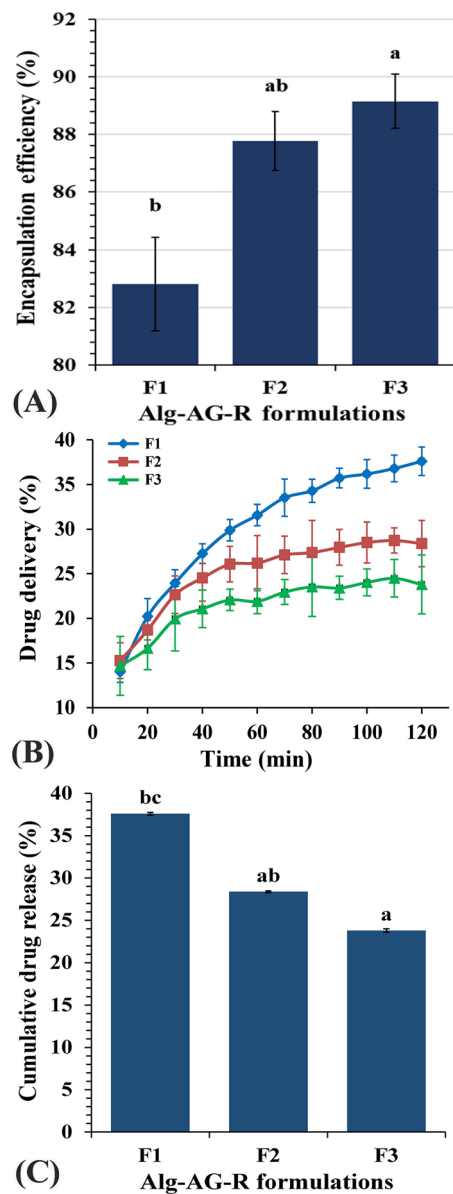


Figure 7. (A) Encapsulation efficiency of riboflavin alginate-Arabic gum formulations, (B) In vitro riboflavin release from riboflavin entrapped Alg-AG beads, (C) Cumulative drug release percent.

continued for 50 min only then a stationary one operated to the end of the experiment. Results indicate that Alg-AG-R 0.1 formulation exhibits the highest R release. After 2 h, Fig. 7C showed different patterns of cumulative drug release (%) profiles of riboflavin with the following hierarchy Alg-AG-R 0.1 (37.598%) > Alg-AG-R 0.15 (28.375%) > Alg-AG-R 0.2 (23.802%). Increments in R release from Alg-AG-R was parallel to increasing alginate content and to decreasing Arabic gum content in the beads on the other side.

The current results indicated that riboflavin release rate significantly increased with decreasing Arabic gum incorporated concentration i.e., by the relative increasing alginate concentration. Owing to interpretation of Peppas and Narasimhan⁷⁶, drug molecules dissolution from polymeric blends depends generally on two key phenomena. Firstly, decomposing of the encapsulating substance and dispersion of the drug molecules through the polymeric matrix; however, the second phenomenon concerned with swelling, chemical decomposition, osmotic consequences. Based on Bera et al.⁷⁷ interpretations, slow prolonged release could be ultimately due to the residual drug that is dispersed in Arabic gum pockets of the beads formulating a drug-Arabic gum dispersed matrix. Consequently, R delivery from Alg-AG-R beads to the dissociation medium may exhibit two steps, including the diffusion of the drug out of Arabic gum pockets into the barium alginate matrix at first, then it could be distributed outwards barium alginate matrix into the dissociation medium. Another point of view was suggested by Bera et al.⁷⁷ who described the behavior of R release to additional Arabic gum barrier formation.

Beirão-da-Costa et al.⁷⁸ documented the importance of alginate volume expansion in the initial exponential phase of R release from Alg-AG matrix. Helrich⁷⁹ suggested that drug release from microparticles might be occurred by different modes of action comprising surface erosion, disintegration, diffusion and desorption. According to Anitha et al.⁸⁰, the initial fast release rate could be attributed to riboflavin molecules adsorption onto and near the particle surface where the alginate dissolution rate is high. Hosseini et al.⁸¹ and Siepmann et al.⁸² documented an alternative interpretation, that slow R delivery during second stage might be attributed to the continuous diffusion of R into Alg-AG microbeads with time, in addition to the maintenance of almost-linear R concentration gradients over extended periods within the Alg-AG microbeads. Alginate microparticles were considered safe, Abdelaziz et al.⁸³ reported alginate nanoparticles as a safe delivery system for miltefosine in the treatment of candidiasis and cryptococcosis. Alginate nanoparticles toxicity were assessed on red blood cells and *Galleria mellonella* larvae. Miltefosine in alginate nanoparticles existed neither hemolytic effect, nor, toxicity in larvae. Results showed the nontoxic use of alginate-based drug-delivery systems as carriers to control the fungal infection in the in vivo model of *G. mellonella*¹⁹. Shanmuganathan et al.⁸⁴ found that various drugs and nanoparticles have been encapsulated or adhered over chitosan nanoparticles and applied for cancer treatment.

Kinetic studies. The mathematical kinetic models: zero order (Supplementary Fig. S3A), first order (Supplementary Fig. S3B), Higuchi (Supplementary Fig. S3C) and Korsmeyer–Peppas (Supplementary Fig. S3D) models were followed for evaluating the in vitro riboflavin release. The zero-order kinetic model is a relation between time (min) and log cumulative percent of drug release, achieving R^2 values ranging from 0.8823 to 0.7914. The first order kinetic model is a relation between time (min) and $\ln(1-F)$, giving R^2 values ranging from 0.777 to 0.7915. Higuchi model is a relation between $t_{1/2}$ and log cumulative percent of drug release achieving R^2 results range of 0.9616 to 0.8945. Korsmeyer Peppas model is a relation between $\ln t$ and log cumulative percent of drug release giving R^2 results range of 0.9783 to 0.9484. The resulted kinetic parameters of curve fitting in the previously mentioned mathematical models are listed in Table 1. Investigating data of corresponding correlation coefficients (R^2) of Alg-AG-R microbeads in the dissociation medium indicated that riboflavin release follows Higuchi model ($R^2 = 0.962\text{--}0.887$) and Korsmeyer Peppas model ($R^2 = 0.948\text{--}0.978$) over a period of 2 h.

Different riboflavin preparations release behavior was assessed using Korsmeyer–Peppas model (Supplementary Fig. S3D) which differentiate between different release mechanisms: Fickian release (controlled release), non-Fickian release (irregular transport), and case-II transport (relaxation-controlled release). Value of $n \leq 0.43$ designates Fickian release, n value range between 0.43 and 0.85 indicates non-Fickian release, Whereas, $n \geq 0.85$, it is case-II transport which includes polymer disbanding and enlargement of polymeric chain⁸⁵. The present data indicate Fickian release (diffusion-controlled release) (n ranges from 0.204 to 0.389) as reported by Siepmann et al.⁸². In accordance with our results, Azad et al.⁷³ reports that the black seed oil release from alginate fitted with Korsmeyer–Peppas kinetic model ($R^2 = 0.900$ to 0.997) over two h period, except for the release exponent (n) values which were in the range of 0.49 to 0.61, designating non-Fickian diffusion in acidic media (pH 1.2). According to the interpretation of Danarto et al.⁸⁶, the ability to encapsulate riboflavin in the alginate–gum Arabic hydrogel could be contributed to the development of an "eggbox" structure during the crosslinking process with Ba^{2+} ions. They suggested that higher sodium-alginate concentration will result in more loading of riboflavin. This might be attributed to the number of "egg-box" structures that are formed within the alginate molecule whereas 3% Na-alginate concentration was the optimum for the loading process.

Materials and methods

Collection and preparation of macroalgal sample. *Sargassum latifolium* (Turner), C. Agardh was collected from the shores of Safaga-Quaser, Red Sea Governorate, Egypt, on June 2017, following the institutional, national and international guidelines and legislation. The macroalga was kindly identified by prof. Dr. Mohamed S. Abdel-Kareem, Botany and Microbiology Department, Faculty of Science, Alexandria University, Egypt. The voucher specimen (*Sargassum latifolium*—Herb. Nasr—1ph-2021) has been deposited at the herbarium of late professor Abdel-Halim Nasr at Botany and Microbiology Department, Faculty of Science, Alexandria University, Egypt. *Sargassum latifolium* thalli were surface cleaned using distilled water, then dried at 60 °C until reaching constant weight. Thereafter, thalli were crushed into small pieces (0.1–0.5 cm)⁸⁷.

Extraction of sodium alginate. Alginate extraction was conducted following Bouissil et al.²⁴ protocol with some modifications. 20 g crushed algal biomass was washed with 300 mL boiling distilled water for 30 min. Then the algal biomass was boiled with 300 mL of 0.5% CaCl_2 solution for 30 min. Afterward, algal residue was obtained and boiled with 300 mL of 0.5% NaCl for 1 h. After filtration the algal sample was boiled with 100 mL of Na_2CO_3 (5%) for 30 min with intensive stirring. After filtration, sodium alginate was precipitated by dehydration using 80% ethyl alcohol and then dried at 50 °C and crushed before storage. Alginate yield was presented as a weight percentage of algal dry biomass according to Belatmania et al.²².

Chemical composition. Total carbohydrates content was estimated according to the method of Farmer et al.⁶⁵ whereas soluble protein was determined following Idrees et al.⁸⁸ protocol. Lipid content was assessed gravimetrically using chloroform–methanol system following the protocol of Currie and Turvey⁸⁹. Sulfate content was assessed after hydrolysis of alginate with 2 M HCl for 2 h at 100 °C according to Association et al.⁹⁰. Uronic acid content was evaluated following the protocol of Blumenkrantz et al.⁹¹. An alginate specimen was added to a solution of sodium tetraborate in concentrated H_2SO_4 , followed by addition of m-hydroxydiphenyl reagent with shaking. The indicative color was developed within 5 min and measured spectrophotometrically at 520 nm.

UV–VIS spectroscopy. The UV–Vis absorbance spectrum of *Sargassum latifolium*-derived alginate solution was recorded using ATI UNICAM-UV/Visible spectrophotometer vision software V3.20 – England in the range of 200–800 nm in the Unit of Spectra – Faculty of Sciences – Mansoura University – Egypt.

¹H NMR spectroscopy. ¹H NMR spectroscopy is a good method for detecting the composition, beside reviewing the block structure of the extracted alginate²². Alginate sample solution (6 mg/mL Deuterium water) was used for ¹H NMR analysis using ECA 500 II (JEOL—Japan) NMR spectrophotometer in the NMR Unit—Faculty of Sciences—Mansoura University—Egypt. The ¹H NMR results were measured using field strength 500 MHz.

Fourier-transform infrared (FTIR) spectroscopy. Dried alginate sample (1 mg) was dispersed and pressed in 0.1 g anhydrous potassium bromide. Spectra of IR were documented at room temperature in the frequency range 400–4000 cm⁻¹⁹² using Mattson 5000—Japan FTIR spectrometer in the Unit of spectra—Faculty of Sciences—Mansoura University—Egypt.

Rheological measurements. Rheological characterization of the alginate extract was performed in the concentrations of 5, 10 and 15 mg/mL using the BROOKFIELD DV-3-USA Ultra Programmable Rheometer in the physics department—Faculty of Science—Mansoura university—Egypt that measures fluid parameters of shear stress and viscosity at given shear rates at 25°C⁹³. Shear stress and viscosity were documented as a function of practical shear rate (10–500 s⁻¹). All rheological data were achieved in triplicate and the mean of values were calculated.

X-ray diffraction (XRD). The X-ray diffraction data of sodium alginate were measured using SHIMADZU-6000—Japan Diffractometer in The Egyptian Atomic Energy Authority. Measurement conditions were, the X-ray tube with Cu anode target, a voltage of 40 kV, and a current of 30 mA. XRD diffractograms were recorded in the 2θ range of 4.0–90 in continuous scan mode with speed of 8.0 deg/min.

Thermogravimetric analysis (TGA). Thermogravimetry (TG), is an analysis by which the change in a specimen mass exposed to progressive heating with a constant rate is documented and illustrated vs. temperature, is an efficient protocol for investigating the thermal stability of a compound. TGA of sodium alginate was performed using a TGA-50 SHIMADZU—Japan Thermogravimetric analyzer at Egyptian Atomic Authority. The process was conducted in the temperature range 20–800°C at a heating rate of 10°C min⁻¹ in nitrogen atmosphere. Data were expressed as percent of mass loss (Δ mass %) versus temperature.

Growth responses of *C. vulgaris* to alginate hydrolysate supplementation. Alginate hydrolysate was prepared according to the protocol of Hotchkiss et al.⁹⁴, with some modifications. Sodium alginate solution (1%) was acidified with 2 mL of 0.2 N HCl and autoclaved at 121°C for 20 min. Then cooled and neutralized using sodium carbonate. Finally, a homologous extract of oligo-guluronic acid was obtained.

Chlorella vulgaris, the test microalga, was provided from the microalgal collection of Phycology Laboratory—Faculty of Science—Mansoura University. *C. vulgaris* was grown up in axenic cultures and incubated for 14 days at 25 ± 2°C under constant illumination (59.4 μmol s⁻¹ m⁻²) using BG11 media⁹³. *C. vulgaris* was grown under a mixotrophic mode of nutrition using alginate hydrolysate as an external carbon source in the following concentrations (0.05, 0.1, 0.3 and 0.5 g/L) to investigate *C. vulgaris* growth and metabolism. Dry biomass was estimated at two days intervals. Moreover, at the end of the experiment, light harvesting pigments, protein as well as carbohydrate contents were estimated as previously mentioned. Photosynthetic pigments (chlorophylls and carotenoids) were assessed following the method of Metzner et al.⁹⁵. Soluble phenols content was assessed according to the method of Gillespie et al.⁹⁶, guaiacol peroxidase (GPX) activity was estimated following the protocol of Curtis et al.⁹⁷.

Sodium alginate as a carrier matrix for riboflavin drug delivery in simulated gastric juice. For preparing Arabic gum-entrapped barium alginate beads loaded with riboflavin (Alg-AG-R), the emulsion-gelation method of Lin et al.⁹⁸ was followed. Two grams of sodium alginate were dissolved in 100 mL deionized water with stirring. Liquid Arabic gum (0.1, 0.15 and 0.2 g) and riboflavin (5 mg) were mixed with the previously prepared sodium alginate solutions, then aqueous preparations of sodium alginate and liquid Arabic gum with riboflavin were stirred for 30 min at 150 rpm for emulsion stability. For producing spherical beads, the formed polymeric emulsion was dropped through glass syringe with a size-22 disposable needle into BaCl₂ solution (1 g BaCl₂ in 100 mL of 10% acetic acid) with continuous stirring. For strengthening the beads, they were permitted to stand for 15 min in the BaCl₂ solution, then filtered and washed twice with deionized water. The resulted beads formulations are Alg-AG-R 0.1 (F1), Alg-AG-R 0.15 (F2), Alg-AG-R 0.2 (F3), Alg-AG 0.1 (F4), Alg-AG 0.15 (F5) and Alg-AG 0.2 (F6), illustrated in Table 2.

The simulated gastric fluid was prepared by dissolving 3.5 g glucose, 2.05 g NaCl, 0.60 g KH₂PO₄, 0.11 g CaCl₂, 0.37 KCl in 200 mL deionized water. The pH of the solution was adjusted to 2 using 1 M HCl and to final volume of 1 L.

Scanning electron microscopy (SEM). The morphology and surface of the alginate beads were assessed using scanning electron microscope (JEOL JSM 6510/V, Japan) at the Electron Microscope Unit, Mansoura University—Egypt.

Formulation	Alginate (g/100 mL)	Arabic gum (g/100 mL)	Riboflavin (mg/100 mL)	Abbreviation
F1	2	0.1	5	Alg-AG-R 0.1
F2	2	0.15	5	Alg-AG-R 0.15
F3	2	0.2	5	Alg-AG-R 0.2
F4	2	0.1	–	Alg-AG 0.1
F5	2	0.15	–	Alg-AG 0.15
F6	2	0.2	–	Alg-AG 0.2

Table 2. Various Alginate- Arabic gum formulations with and without riboflavin.

Model	Formula	Constant
Zero-order model	$F = K_0 t$	K_0
First-order model	$\ln(1 - F) = -K_{1st} t$	K_{1st}
Higuchi Model	$F = K_H t^{1/2}$	K_H
Korsmeyer-Peppas model	$F = K_p t^n$	K_p

Table 3. Kinetic models applied on riboflavin release from R-Alg-AG beads.

In vitro release studies of riboflavin. The in vitro release of riboflavin drug from different liquid Arabic gum-entrapped barium alginate beads formulations was investigated for 120 min with regular time intervals. Different Arabic gum—entrapped barium alginate beads formulations loaded with riboflavin were added to the simulated gastric fluid with stirring (50 rpm) at 35 ± 2 °C. For investigating riboflavin release, sampling solution aliquots at 10 min intervals were used to estimate riboflavin concentration spectrophotometrically at 444 nm using riboflavin standard curve. Encapsulation efficiency percent (EE %) was determined following the equation of Nallasamy et al.⁹⁹

$$EE(\%) = \frac{\text{total amount of loaded R}}{\text{initial amount of R}} \times 100 \quad (1)$$

Riboflavin release kinetics. For interpreting the performance of riboflavin release from the barium alginate beads in simulated gastric fluid (pH 2), suitable mathematical models must be followed. In vitro riboflavin release from different alginate-Arabic gum beads loaded with riboflavin (Alg-AG-R) data were assessed kinetically through different mathematical models: (Zero-order, First-order, Higuchi and Korsmeyer-Peppas model)¹⁰⁰ as shown in Table 3; where F represents the drug fraction released at time t, K_0 represents zero-order release constant, K_1 represents the first-order release constant, K_H represents Higuchi dissolution constant and K_p is Korsmeyer-Peppas constant and n represents the release exponent.

Statistical analysis. Data were subjected to statistical analysis following Zobel et al.¹⁰¹ using one-way analysis of variance followed by least significant difference (LSD) analysis, P-values more than 0.05 were considered statistically, non-significant, whereas P-value less than 0.05 represent statistically significant data. Results were expressed as mean \pm standard deviation.

Conclusion

In this study, *Sargassum latifolium*—derived alginate hydrolysate can be used as *C. vulgaris* growth bio-stimulant. A new sustained release system of riboflavin-entrapped barium alginate-Arabic gum drug delivery matrix was elucidated. Moreover, drug entrapment technique using alginate is a valuable developmental tool of the multi particulate system for drug delivery even for a highly water-soluble drug such as riboflavin.

Received: 31 March 2021; Accepted: 4 August 2021

Published online: 18 August 2021

References

1. Veluchamy, C. & Palaniswamy, R. A review on marine algae and its applications. *Asian J. Pharm. Clin. Res.* **13**, 21–27 (2020).
2. Ganesan, A. R., Tiwari, U. & Rajauria, G. Seaweed nutraceuticals and their therapeutic role in disease prevention. *Food Sci. Hum. Wellness* **8**, 252–263 (2019).
3. Martínez-Gómez, F., Guerrero, J., Matsuhiro, B. & Pavez, J. Characterization of poly-D-mannuronate and poly-L-gulonate block fractions from sodium alginate and preparation of hydrogels with poly(vinylalcohol). *Int. J. Biol. Macromol.* **111**, 935–946 (2018).
4. Eskens, O., Villani, G. & Amin, S. Rheological investigation of thermoresponsive alginate-methylcellulose gels for epidermal growth factor formulation. *Cosmetics* **8**, 1–11 (2021).
5. Berg, A., Droegge, M. W., Fellmann, J. D., Klaveness, J. & Rongved, P. Medical use of organic aerogels and biodegradable organic aerogels. *WO Pat.* **95**, 1165 (1995).

6. Ulker, Z. & Erkey, C. An advantageous technique to load drugs into aerogels: Gas antisolvent crystallization inside the pores. *J. Supercrit. Fluids* **120**, 310–319 (2017).
7. García-González, C. A., Jin, M., Gerth, J., Alvarez-Lorenzo, C. & Smirnova, I. Polysaccharide-based aerogel microspheres for oral drug delivery. *Carbohydr. Polym.* **117**, 797–806 (2015).
8. Iwamoto, M. *et al.* Structure–activity relationship of alginate oligosaccharides in the induction of cytokine production from RAW264.7 cells. *FEBS Lett.* **579**, 4423–4429 (2005).
9. Schafer, D. P. *et al.* Microglia sculpt postnatal neural circuits in an activity and complement-dependent manner. *Neuron* **74**, 691–705 (2012).
10. Josephine, A. *et al.* Analytical evaluation of different carbon sources and growth stimulators on the biomass and lipid production of *Chlorella vulgaris*—Implications for biofuels. *Biomass Bioenerg.* **75**, 170–179 (2015).
11. Chu, H.-Q. *et al.* Continuous cultivation of *Chlorella pyrenoidosa* using anaerobic digested starch processing wastewater in the outdoors. *Bioresour. Technol.* **185**, 40–48 (2015).
12. Sung, K.-D., Lee, J.-S., Shin, C.-S., Park, S.-C. & Choi, M.-J. CO₂ fixation by *Chlorella* sp. KR-1 and its cultural characteristics. *Bioresour. Technol.* **68**, 269–273 (1999).
13. Dalrymple, O. K. *et al.* Wastewater use in algae production for generation of renewable resources: A review and preliminary results. *Aquat. Biosyst.* **9**, 1–11 (2013).
14. GVNS, D., Pradeep, K. V & Prasuna, R. G. Pelagia research library. *Eur. J. Exp. Biol.* **1**, 216–222 (2011).
15. Li, Y., Yang, H. Y. & Lee, D. S. Advances in biodegradable and injectable hydrogels for biomedical applications. *J. Control. Release* **330**, 151–160 (2020).
16. Hill, M. *et al.* Alginate/chitosan particle-based drug delivery systems for pulmonary applications. *Pharmaceutics* **11**, 1–12 (2019).
17. Chan, E.-S., Yim, Z.-H., Phan, S.-H., Mansa, R. F. & Ravindra, P. Encapsulation of herbal aqueous extract through absorption with ca-alginate hydrogel beads. *Food Bioprod. Process.* **88**, 195–201 (2010).
18. Choukaife, H., Doolaanea, A. A. & Alfatama, M. Alginate nanoformulation: Influence of process and selected variables. *Pharmaceutics* **13**, 1–35 (2020).
19. Hariyadi, D. M. & Islam, N. Current status of alginate in drug delivery. *Adv. Pharmacol. Pharm. Sci.* **2020**, 1–16 (2020).
20. Li, J., Jia, X. & Yin, L. Hydrogel: Diversity of structures and applications in food science. *Food Rev. Int.* **37**, 313–372 (2021).
21. Chandia, N. P., Matsuhiro, B., Mejias, E. & Moenne, A. Alginic acids in *Lessonia vadosa*: partial hydrolysis and elicitor properties of the polymannuronic acid fraction. *J. Appl. Phycol.* **16**, 127–133 (2004).
22. Belattmania, Z. *et al.* Isolation and FTIR-ATR and ¹H NMR characterization of alginates from the main alginophyte species of the Atlantic Coast of Morocco. *Molecules* **25**, 4335 (2020).
23. Mohammed, A., Rivers, A., Stuckey, D. C. & Ward, K. Alginate extraction from *Sargassum* seaweed in the Caribbean region: Optimization using response surface methodology. *Carbohydr. Polym.* **245**, 116419 (2020).
24. Bouissil, S. *et al.* Use of alginate extracted from Moroccan brown algae to stimulate natural defense in date palm roots. *Molecules* **25**, 720 (2020).
25. Larsen, C. K., Gåserød, O. & Smidsrød, O. A novel method for measuring hydration and dissolution kinetics of alginate powders. *Carbohydr. Polym.* **51**, 125–134 (2003).
26. Duarte, M. E. R., Cardoso, M. A., Nosedá, M. D. & Cerezo, A. S. Structural studies on fucoidans from the brown seaweed *Sargassum stenophyllum*. *Carbohydr. Res.* **333**, 281–293 (2001).
27. Goma, M., Fawzy, M. A., Hifney, A. F. & Abdel-Gawad, K. M. Use of the brown seaweed *Sargassum latifolium* in the design of alginate-fucoidan based films with natural antioxidant properties and kinetic modeling of moisture sorption and polyphenolic release. *Food Hydrocolloids* **82**, 64–72 (2018).
28. Viswanathan, S. & Nallamuthu, T. Extraction of sodium alginate from selected seaweeds and their physicochemical and biochemical properties. *Extraction* **3**, 10998–11003 (2014).
29. Osman, M. E., Menzies, A. R., Williams, P. A., Phillips, G. O. & Baldwin, T. C. The molecular characterisation of the polysaccharide gum from *Acacia senegal*. *Carbohydr. Res.* **246**, 303–318 (1993).
30. Rajeswari, R. & Jayaprakash, K. Bioactive potential analysis of brown seaweed *Sargassum wightii* using UV-VIS and FT-IR. *J. Drug Deliv. Ther.* **9**, 150–153 (2019).
31. Hussein, M. H. *et al.* Characterization and chromium biosorption potential of extruded polymeric substances from *Synechococcus mundulus* induced by acute dose of gamma irradiation. *Environ. Sci. Pollut. Res.* **26**, 31998–32012 (2019).
32. Usoltseva, R. V. *et al.* Comparison of structure and in vitro anticancer activity of native and modified fucoidans from *Sargassum feldmannii* and *S. duplicatum*. *Int. J. Biol. Macromol.* **124**, 220–228 (2019).
33. Holtan, S., Zhang, Q., Strand, W. I. & Skjåk-Bræk, G. Characterization of the hydrolysis mechanism of polyalternating alginate in weak acid and assignment of the resulting MG-oligosaccharides by NMR spectroscopy and ESI– mass spectrometry. *Bio-macromol* **7**, 2108–2121 (2006).
34. Trica, B. *et al.* Extraction and characterization of alginate from an edible brown seaweed (*Cystoseira barbata*) harvested in the Romanian Black Sea. *Mar. Drugs* **17**, 405 (2019).
35. Flórez-Fernández, N., Domínguez, H. & Torres, M. D. A green approach for alginate extraction from *Sargassum muticum* brown seaweed using ultrasound-assisted technique. *Int. J. Biol. Macromol.* **124**, 451–459 (2019).
36. Aprilliza, M. Characterization and properties of sodium alginate from brown algae used as an ecofriendly superabsorbent. in *IOP Conference Series: Materials Science and Engineering*. **188**, 12019 (2017).
37. Stojanovic, R. *et al.* Encapsulation of thyme (*Thymus serpyllum* L.) aqueous extract in calcium alginate beads. *J. Sci. Food Agric.* **92**, 685–696 (2012).
38. Rahiminezhad, Z., Tamaddon, A. M., Borandeh, S. & Abolmaali, S. S. Janus nanoparticles: New generation of multifunctional nanocarriers in drug delivery, bioimaging and theranostics. *Appl. Mater. Today* **18**, 100513 (2020).
39. Carpenter, J. & Saharan, V. K. Ultrasonic assisted formation and stability of mustard oil in water nanoemulsion: Effect of process parameters and their optimization. *Ultrason. Sonochem.* **35**, 422–430 (2017).
40. Cardenas-Jiron, G., Leal, D., Matsuhiro, B. & Osorio-Roman, I. O. Vibrational spectroscopy and density functional theory calculations of poly-D-mannuronate and heteropolymeric fractions from sodium alginate. *J. Raman Spectrosc.* **42**, 870–878 (2011).
41. Guedes Soares, C., Cherneva, Z. & Antao, E. M. Abnormal waves during hurricane Camille. *J. Geophys. Res. Ocean.* **109**, 1–7 (2004).
42. Rani, P. L. *et al.* Influence of dates of sowing and nitrogen levels on growth and yield of Kharif maize under irrigated conditions in South Telanagana Agro-climatic Zone of Andhra Pradesh, India. *Int. J. Bio-resource Stress Manag.* **4**, 34–42 (2013).
43. dos Santos Araújo, P., Belini, G. B., Mambrini, G. P., Yamaji, F. M. & Waldman, W. R. Thermal degradation of calcium and sodium alginate: A greener synthesis towards calcium oxide micro/nanoparticles. *Int. J. Biol. Macromol.* **140**, 749–760 (2019).
44. Xu, S., Tabaković, A., Liu, X., Palin, D. & Schlangen, E. Optimization of the calcium alginate capsules for self-healing asphalt. *Appl. Sci.* **9**, 1–12 (2019).
45. Manjuladevi, M., Anitha, R. & Manonmani, S. Kinetic study on adsorption of Cr (VI), Ni (II), Cd (II) and Pb (II) ions from aqueous solutions using activated carbon prepared from *Cucumis melo* peel. *Appl. Water Sci.* **8**, 1–8 (2018).
46. Kanimozhi, K., Basha, S. K., Kumari, V. S., Kaviyarasu, K. & Maaza, M. *In vitro* cytocompatibility of chitosan/PVA/methylcellulose–Nanocellulose nanocomposites scaffolds using L929 fibroblast cells. *Appl. Surf. Sci.* **449**, 574–583 (2018).

47. Sabet, S. *et al.* The interactions between the two negatively charged polysaccharides: Gum Arabic and alginate. *Food Hydrocoll.* **112**, 106343 (2021).
48. Wildemuth, C. R. & Williams, M. C. Viscosity of suspensions modeled with a shear-dependent maximum packing fraction. *Rheol. Acta* **23**, 627–635 (1984).
49. Shyamali, S. Carbohydrate constituents of the marine algae of Sri Lanka. 2. Composition and sequence of urinate residues in alginates from some brown seaweeds. *J. Nat. Sci. Counc. Sri Lanka* **12**, 161–166 (1984).
50. Glicksman, M. Gum Technology in the Food Industry/Martin Glicksman. Vol. **11**, 895–902 (1969).
51. Truus, K. *et al.* The content of micro- and trace elements in commercial agaroses and their raw material. *Proc. Est. Acad. Sci. Chem* **42**, 87–96 (1993).
52. Picout, D. R. & Ross-Murphy, S. B. Rheology of biopolymer solutions and gels. *Sci. World J.* **3**, 105–121 (2003).
53. Bhatnagar, M., Pareek, S., Ganguly, J. & Bhatnagar, A. Rheology and composition of a multi-utility exopolymer from a desert borne cyanobacterium *Anabaena variabilis*. *J. Appl. Phycol.* **24**, 1387–1394 (2012).
54. Freitas, F. *et al.* Emulsifying behaviour and rheological properties of the extracellular polysaccharide produced by *Pseudomonas oleovorans* grown on glycerol byproduct. *Carbohydr. Polym.* **78**, 549–556 (2009).
55. Khattar, J. I. S. *et al.* Isolation and characterization of exopolysaccharides produced by the cyanobacterium *Limnithrix redekei* PUPCCC 116. *Appl. Biochem. Biotechnol.* **162**, 1327–1338 (2010).
56. Sutherland, I. W. *Biotechnology of Microbial Exopolysaccharides* (Cambridge University Press, 1990).
57. Shen, X. F. *et al.* Biodiesel production from *Chlorella vulgaris* under nitrogen starvation in autotrophic, heterotrophic, and mixotrophic cultures. *J. Appl. Phycol.* **31**, 1589–1596 (2019).
58. Yokose, T. *et al.* Growth-promoting effect of alginate oligosaccharides on a unicellular marine microalga, *Nannochloropsis oculata*. *Biosci. Biotechnol. Biochem.* **73**, 450–453 (2009).
59. Yamasaki, Y. *et al.* Effects of alginate oligosaccharide mixtures on the growth and fatty acid composition of the green alga *Chlamydomonas reinhardtii*. *J. Biosci. Bioeng.* **113**, 112–116 (2012).
60. Yokose, N. *et al.* Bedside monitoring of cerebral blood oxygenation and hemodynamics after aneurysmal subarachnoid hemorrhage by quantitative time-resolved near-infrared spectroscopy. *World Neurosurg.* **73**, 508–513 (2010).
61. Ueno, M. & Oda, T. Effects of alginate oligosaccharides on the growth of marine microalgae. In *Mar. Algae Extr. Process. Prod. Appl.* 213–226 (2015).
62. Naeem, M., Idrees, M., Aftab, T., Khan, M. M. A. & Varshney, L. Irradiated sodium alginate improves plant growth, physiological activities and active constituents in *Mentha arvensis* L.. *J. Appl. Pharm. Sci.* **2**, 28 (2012).
63. El-Chaghaby, G. A., Rashad, S., Abdel-Kader, S. F., Rawash, E.-S.A. & Abdul Moneem, M. Assessment of phytochemical components, proximate composition and antioxidant properties of *Scenedesmus obliquus*, *Chlorella vulgaris* and *Spirulina platensis* algae extracts. *Egypt. J. Aquat. Biol. Fish.* **23**, 521–526 (2019).
64. Abd El-Rehim, H. A. Characterization and possible agricultural application of polyacrylamide/sodium alginate crosslinked hydrogels prepared by ionizing radiation. *J. Appl. Polym. Sci.* **101**, 3572–3580 (2006).
65. Farmer, E. E., Moloshok, T. D., Saxton, M. J. & Ryan, C. A. Oligosaccharide signaling in plants. Specificity of oligouronide-enhanced plasma membrane protein phosphorylation. *J. Biol. Chem.* **266**, 3140–3145 (1991).
66. Malakar, J., Nayak, A. K. & Pal, D. Development of cloxacillin loaded multiple-unit alginate-based floating system by emulsion–gelation method. *Int. J. Biol. Macromol.* **50**, 138–147 (2012).
67. Rashidzadeh, B. *et al.* Preparation and characterization of antibacterial magnetic-/pH-sensitive alginate/Ag/Fe₃O₄ hydrogel beads for controlled drug release. *Int. J. Biol. Macromol.* **154**, 134–141 (2020).
68. Al-Tahami, K. Preparation, characterization, and in vitro release of ketoprofen loaded alginate microspheres. *Int. J. App. Pharm.* **6**, 9–12 (2014).
69. Sinha, S., Astani, A., Ghosh, T., Schnitzler, P. & Ray, B. Polysaccharides from *Sargassum tenerrimum*: structural features, chemical modification and anti-viral activity. *Phytochemistry* **71**, 235–242 (2010).
70. Sari-Chmayssem, N. *et al.* Extracted and depolymerized alginates from brown algae *Sargassum vulgare* of Lebanese origin: Chemical, rheological, and antioxidant properties. *J. Appl. Phycol.* **28**, 1915–1929 (2016).
71. Hosseini, S. F., Zandi, M., Rezaei, M. & Farahmandghavi, F. Two-step method for encapsulation of oregano essential oil in chitosan nanoparticles: Preparation, characterization and in vitro release study. *Carbohydr. Polym.* **95**, 50–56 (2013).
72. Gouin, S. Microencapsulation: Industrial appraisal of existing technologies and trends. *Trends Food Sci. Technol.* **15**, 330–347 (2004).
73. Azad, A. K. *et al.* Encapsulation of black seed oil in alginate beads as a pH-sensitive carrier for intestine-targeted drug delivery: *In vitro*, *in vivo* and *ex vivo* study. *Pharmaceutics* **12**, 219 (2020).
74. Piornos, J. A., Burgos-Díaz, C., Morales, E., Rubilar, M. & Acevedo, F. Highly efficient encapsulation of linseed oil into alginate/lupin protein beads: Optimization of the emulsion formulation. *Food Hydrocoll.* **63**, 139–148 (2017).
75. Schulz, A. *et al.* Poly (amidoamine)-alginate hydrogels: directing the behavior of mesenchymal stem cells with charged hydrogel surfaces. *J. Mater. Sci. Mater. Med.* **29**, 1–13 (2018).
76. Peppas, N. A. & Narasimhan, B. Mathematical models in drug delivery: How modeling has shaped the way we design new drug delivery systems. *J. Control. Release* **190**, 75–81 (2014).
77. Bera, R. *et al.* Formulation and in vitro evaluation of sunflower oil entrapped within buoyant beads of furosemide. *Sci. Pharm.* **77**, 669–678 (2009).
78. Beirão-da-Costa, S. *et al.* Inulin potential for encapsulation and controlled delivery of Oregano essential oil. *Food Hydrocoll.* **33**, 199–206 (2013).
79. Helrich, K. *Official Methods of Analysis of the Association of Official Analytical Chemists*. Association of official analytical chemists (1990).
80. Anitha, A. *et al.* Preparation, characterization, in vitro drug release and biological studies of curcumin loaded dextran sulphate–chitosan nanoparticles. *Carbohydr. Polym.* **84**, 1158–1164 (2011).
81. Hosseini, S. M. *et al.* Incorporation of essential oil in alginate microparticles by multiple emulsion/ionic gelation process. *Int. J. Biol. Macromol.* **62**, 582–588 (2013).
82. Siepmann, J., Faisant, N., Akiki, J., Richard, J. & Benoit, J. P. Effect of the size of biodegradable microparticles on drug release: Experiment and theory. *J. Control. Release* **96**, 123–134 (2004).
83. Abdelaziz, H. M. *et al.* Inhalable particulate drug delivery systems for lung cancer therapy: Nanoparticles, microparticles, nanocomposites and nanoaggregates. *J. Control. Release* **269**, 374–392 (2018).
84. Shanmuganathan, R. *et al.* Chitosan nanopolymers: An overview of drug delivery against cancer. *Int. J. Biol. Macromol.* **130**, 727–736 (2019).
85. Djoullah, A., Djemaoune, Y., Husson, F. & Saurel, R. Native-state pea albumin and globulin behavior upon transglutaminase treatment. *Process Biochem.* **50**, 1284–1292 (2015).
86. Danarto, Y. C., Rochmadi & Budhijanto. Microencapsulation of riboflavin (vitamin B2) using alginate and chitosan: Effect of alginate and chitosan concentration upon encapsulation efficiency. *IOP Conf. Ser. Mater. Sci. Eng.* **858**, 1–6 (2020).
87. Prabhu, R. *et al.* Ecofriendly one pot fabrication of methyl gallate@ZIF-L nanoscale hybrid as pH responsive drug delivery system for lung cancer therapy. *Process Biochem.* **84**, 39–52 (2019).

88. Idrees, M. *et al.* Utilizing the γ -irradiated sodium alginate as a plant growth promoter for enhancing the growth, physiological activities, and alkaloids production in *Catharanthus roseus* L.. *Agric. Sci. China* **10**, 1213–1221 (2011).
89. Currie, A. J. & Turvey, J. R. An enzymic method for the assay of d-mannuronan C-5 epimerase activity. *Carbohydr. Res.* **107**, 156–159 (1982).
90. Association, A. P. H. & Association, A. W. W. *Standard Methods for the Examination of Water and Wastewater* (Am. public Heal. Assoc., 1989).
91. Blumenkrantz, N. & Asboe-Hansen, G. New method for quantitative determination of uronic acids. *Anal. Biochem.* **54**, 484–489 (1973).
92. Hashemi Gahruie, H., Eskandari, M. H., Van der Meeren, P. & Hosseini, S. M. H. Study on hydrophobic modification of basil seed gum-based (BSG) films by octenyl succinate anhydride (OSA). *Carbohydr. Polym.* **219**, 155–161 (2019).
93. El-Naggar, N.E.-A., Hussein, M. H., Shaaban-Dessuuki, S. A. & Dalal, S. R. Production, extraction and characterization of *Chlorella vulgaris* soluble polysaccharides and their applications in AgNPs biosynthesis and biostimulation of plant growth. *Sci. Rep.* **10**, 1–19 (2020).
94. Hotchkiss, A. T. & Hicks, K. B. Analysis of oligogalacturonic acids with 50 or fewer residues by high-performance anion-exchange chromatography and pulsed amperometric detection. *Anal. Biochem.* **184**, 200–206 (1990).
95. Metzner, H., Rau, H. & Senger, H. Untersuchungen zur synchronisierbarkeit einzelner pigmentmangel-mutanten von *Chlorella*. *Planta* **65**, 186–194 (1965).
96. Gillespie, K. M., Chae, J. M. & Ainsworth, E. A. Rapid measurement of total antioxidant capacity in plants. *Nat. Protoc.* **2**, 867–870 (2007).
97. Curtis, C. R. Disc electrophoretic comparisons of proteins and peroxidases from *Phaseolus vulgaris* leaves infected with *Agrobacterium tumefaciens*. *Can. J. Bot.* **49**, 333–337 (1971).
98. Lin, D., Kelly, A. L., Maidannyk, V. & Miao, S. Effect of concentrations of alginate, soy protein isolate and sunflower oil on water loss, shrinkage, elastic and structural properties of alginate-based emulsion gel beads during gelation. *Food Hydrocoll.* **108**, 105998 (2020).
99. Nallasamy, P. *et al.* Polyherbal drug loaded starch nanoparticles as promising drug delivery system: Antimicrobial, antibiofilm and neuroprotective studies. *Process Biochem.* **92**, 355–364 (2020).
100. Karasulu, E., Karasulu, H. Y., Ertan, G., Kirilmaz, L. & Güneri, T. Extended release lipophilic indomethacin microspheres: Formulation factors and mathematical equations fitted drug release rates. *Eur. J. Pharm. Sci.* **19**, 99–104 (2003).
101. Zobel, R. W., Wright, M. J. & Gauch, H. G. Jr. Statistical analysis of a yield trial. *Agron. J.* **80**, 388–393 (1988).

Acknowledgements

All the authors want to offer many thanks to **prof. Dr. Mohamed S. Abdel-Kareem**, Botany and Microbiology Department, Faculty of Science, Alexandria University, Egypt, for identifying the alga used in this manuscript, *Sargassum latifolium*.

Author contributions

S.R.D. carried out the experiments. M.H.H. proposed the research topic, designed the research plan, provided necessary tools for experiments, experimental instructions, collected the data, interpretation of the results, wrote and revised the manuscript. N.E.E. prepared the Tables and Figures, contributed substantially to the reviewing and revising of the manuscript. S.I.M. contributed substantially to the reviewing and revising of the manuscript. S.A.S.D. participated in the manuscript revision. All authors read and approved the final manuscript.

Competing interests

The authors declare no competing interests.

Additional information

Supplementary Information The online version contains supplementary material available at <https://doi.org/10.1038/s41598-021-96202-0>.

Correspondence and requests for materials should be addressed to N.E.-A.E.-N.

Reprints and permissions information is available at www.nature.com/reprints.

Publisher's note Springer Nature remains neutral with regard to jurisdictional claims in published maps and institutional affiliations.



Open Access This article is licensed under a Creative Commons Attribution 4.0 International License, which permits use, sharing, adaptation, distribution and reproduction in any medium or format, as long as you give appropriate credit to the original author(s) and the source, provide a link to the Creative Commons licence, and indicate if changes were made. The images or other third party material in this article are included in the article's Creative Commons licence, unless indicated otherwise in a credit line to the material. If material is not included in the article's Creative Commons licence and your intended use is not permitted by statutory regulation or exceeds the permitted use, you will need to obtain permission directly from the copyright holder. To view a copy of this licence, visit <http://creativecommons.org/licenses/by/4.0/>.

© The Author(s) 2021